Journal of Materials Chemistry A

Accepted Manuscript

ROYAL SOCIETY OF CHEMISTRY

www.rsc.org/materialsA

Journal of Materials Chemistry A

Dynamic Article Links ►

Cite this: DOI: 10.1039/c0xx00000x

PAPER

www.rsc.org/xxxxxx

Enhanced Hydrogen Storage Properties of Mg–Ag Alloy with a Solid Dissolution of Indium: A Comparative Study

Tingzhi Si,[a] Yu Cao,[a] Qingan Zhang,*[a] Dalin Sun,[b] Liuzhang Ouyang,*[c,d] and Min Zhu[c,d]

Received (in XXX, XXX) Xth XXXXXXXXX 20XX, Accepted Xth XXXXXXXXX 20XX

DOI: 10.1039/b000000x

A comparative study of $Mg_{5.7}In_{0.3}Ag$ and Mg_6Ag alloys was conducted to reveal the effects of indium (In) solid solutions on the hydrogen storage properties of Mg-based alloys. Different from the Mg_6Ag alloy, the as-cast $Mg_{5.7}In_{0.3}Ag$ alloy was composed of a Mg(In) solid solution and Mg_3Ag. However, an initial hydrogen absorption/desorption treatment (i.e., activation) propelled the In atoms in Mg(In) toward Mg_3Ag, forming $(Mg, In)_3Ag$ in the activated sample. This transformation involving the dissolution of In atoms from Mg into solid Mg_3Ag not only greatly improved the thermodynamics of hydrogen desorption but also enhanced its catalytic effect on hydrogen desorption from additional MgH_2. The $(Mg, In)_3Ag–H_2$ system exhibited altered thermodynamics, as its enthalpy change of the hydrogen desorption was 62.6 kJ mol^{-1} H_2. Moreover, the activation energy of the hydrogen desorption from the $Mg_{5.7}In_{0.3}Ag$ sample was lowered to 78.2 kJ mol^{-1}.

1. Introduction

Magnesium (Mg) is an abundant, inexpensive and lightweight metal that can store 7.6 wt.% hydrogen. It has thus been deemed as a suitable medium for high-energy, solid-state, reversible hydrogen storage.[1] However, its practical application as a hydrogen storage material has been plagued by sluggish hydrogen absorption/desorption kinetics and high thermostability.[2,3] These drawbacks are mainly attributed to (i) the high activation energy barriers of the dissociation of hydrogen molecules from the Mg surface and hydrogen diffusion into the formed MgH_2[4,5] and (ii) the strong Mg–H ionic bond.[6] To address the aforementioned problems, a simple but effective strategy, i.e., alloying Mg with other elements to form Mg-based compounds[7–13] or solid solutions[14–17], was proposed.

A well-known example of a Mg-based compound is Mg_2Ni, which forms Mg_2NiH_4 upon hydrogenation. It possesses a low enthalpy of hydrogen desorption (ΔH_d = 65 kJ mol^{-1} H_2). Mg_2Cu can also reversibly undergo hydrogenation, but unlike Mg_2Ni, which forms a single hydride (Mg_2NiH_4), it forms two products via disproportionation: $Mg_2Cu + 3/2H_2 \rightarrow 3/2MgH_2 + 1/2MgCu_2$. As such a reaction also exhibits altered thermodynamics (ΔH_d = 70 kJ mol^{-1} H_2),[8] MgH_2 may react with $MgCu_2$ and destabilize, thus forming Mg_2Cu. Similarly, we recently used a reversible $Mg_3Ag–H_2$ system for hydrogen storage through the reaction in Eq. (1), which has a low ΔH_d value (69.8 kJ mol^{-1} H_2).[13]

$$Mg_3Ag + 2H_2 \leftrightarrow 2MgH_2 + MgAg \qquad (1)$$

These studies clearly indicate that alloying Mg with other elements to form Mg-based compounds is an efficient method to improve hydrogen absorption/desorption thermodynamics. However, the aforementioned alloys possess a low capacity for hydrogen.

Generally, preparing Mg-based solid solutions for reversible hydrogen storage is difficult. However, a fully reversible $Mg(In)–H_2$ system with low a ΔH_d value (67.8 kJ mol^{-1} H_2) was realized recently through a reaction between MgH_2 and β-MgIn phases.[16] On the basis of this study, a Mg(In, Y) solid solution and $(Mg, In)_2Ni$ were found to have improved hydrogen absorption/desorption thermodynamics.[18,19] It is therefore of interest to determine whether dissolution of indium in Mg_3Ag can further improve the thermodynamics of the $Mg_3Ag–H_2$ system. However, little work has been done to examine this concept because of the low capacity of Mg_3Ag. In view of the high catalytic activity of Mg-based compounds in hydrogen sorption by pure Mg,[20–24] we used $Mg_{5.7}In_{0.3}Ag$, a magnesium-rich alloy containing Mg_3Ag and Mg phases in the present work to reveal the influence of In on the hydrogen storage thermodynamics of Mg_3Ag and to examine the catalytic activity of Mg–Ag compounds in the presence of additional MgH_2. For comparison, we studied in parallel the hydrogen storage properties of a Mg_6Ag alloy.

2. Experimental section

The alloys Mg_6Ag and $Mg_{5.7}In_{0.3}Ag$ were prepared by induction melting of appropriate amounts of the pure metals under an Ar atmosphere (0.06 MPa). Loss of Mg was determined to be ~16 wt.% from repeated experiments. On the basis of the stoichiometric amounts of the starting materials, an additional 16 wt.% of Mg was added to compensate for the loss of Mg during melting. Samples were remelted three times to ensure homogeneity. To activate them for hydrogen absorption/desorption, the alloys were pulverized and ball-milled for 20 h under an Ar atmosphere by using a planetary mill at a speed of 200 rpm.

The microstructures and phase compositions of the as-cast alloys were examined by scanning electron microscopy (SEM) and energy-dispersive spectrometry (EDS) using a Nova NanoSEM 430 at an accelerating voltage of 20 kV. To evaluate the phase structures of the samples, X-ray diffraction (XRD) measurements were carried out on a Rigaku D/Max 2500VL/PC diffractometer using Cu Kα radiation at 50 kV and 200 mA. The XRD samples were loaded and sealed in a special holder to keep the samples under an argon atmosphere during the course of the measurements. XRD profiles were finally refined by using the Rietveld program RIETAN–2000.[25]

To investigate the properties of hydrogen storage of the alloys, powder samples were loaded into stainless-steel containers which were then placed in stainless-steel autoclaves. The hydrogen absorption and desorption kinetics were monitored at initial hydrogen pressures of 3.0 and 0.001 MPa, respectively, by using an automated Sieverts-type apparatus. To understand the thermodynamic characteristics, pressure–composition (*P*–*C*) isotherms of the samples were obtained at various temperatures. Differential scanning calorimetry (DSC) was conducted on the hydrogenated samples under an argon flow (30 ml min^{-1}) at a heating rate of 2 °C min^{-1} by a Netzsch STA 409 PC/PG unit. Before measurements, the samples were activated by one hydriding/dehydriding cycle at 350 °C. Upon initial cycling, the powder samples were hydrogenated under a hydrogen pressure of 3.0 MPa for 2 h and subsequently evacuated for 2 h.

3. Results and discussion

3.1 Initial hydrogenation and dehydrogenation characteristics during activation

XRD patterns and Rietveld refinement results for the as-cast Mg_6Ag sample and for the samples after the initial hydrogenation and dehydrogenation are shown in Figure 1. It can be seen that the as-cast Mg_6Ag sample was composed of Mg, Mg_4Ag and $Mg_{54}Ag_{17}$ phases. Rietveld analysis results listed in Table 1 further reveal that quantities of the Mg, Mg_4Ag and $Mg_{54}Ag_{17}$ phases were 35, 32 and 33 wt.%, respectively. After full hydrogenation at 350 °C, the Mg, Mg_4Ag and $Mg_{54}Ag_{17}$ phases disappeared, while the MgAg and MgH_2 phases appeared (see Figure 1b), indicating a hydrogen-induced decomposition of the Mg_4Ag and $Mg_{54}Ag_{17}$ phases. Importantly, the MgAg and MgH_2 phases could be converted back to Mg, Mg_4Ag and $Mg_{54}Ag_{17}$ phases at 350 °C (see Figure 1c and Table 1). Therefore, the Mg_6Ag–H_2 system was fully reversible. The hydriding/dehydriding reaction could be expressed as follows:

$$Mg + Mg_4Ag + Mg_{54}Ag_{17} + H_2 \leftrightarrow MgH_2 + MgAg \quad (2)$$

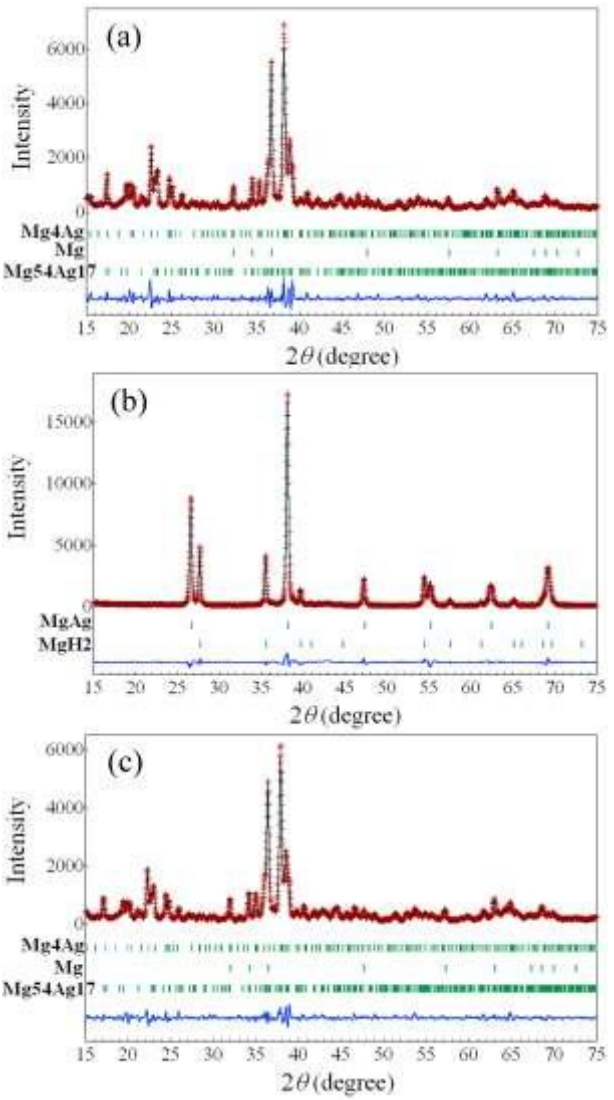

Figure 1 Rietveld refinement results of the observed XRD patterns for the (a) as-cast, (b) hydrogenated, and (c) dehydrogenated Mg_6Ag samples at 350 °C.

After alloying with In, peaks corresponding to a compound of In with Mg or Ag were not detected, and only peaks for Mg (40 wt.%) and Mg_3Ag (60 wt.%) were observed, as shown in Figure 2a and Table 1. These results strongly suggest that Mg and/or Mg_3Ag formed a solid solution with In. To understand the In distribution, SEM/EDS was performed on the as-cast $Mg_{5.7}In_{0.3}Ag$ sample. As shown in Figure 3, a pro-eutectic Mg(In) solid solution (arrow A) was surrounded by eutectic Mg(In)–Mg_3Ag networks (arrow B), indicating that In dissolved in Mg rather than in Mg_3Ag, forming a Mg(In) solid solution.

Table 1 Structural parameters and phase abundance of the as-cast, hydrogenated and dehydrogenated Mg_6Ag and $Mg_{5.7}In_{0.3}Ag$ samples.

Sample	Phase	Space Group	R_I (%)	Lattice Parameters			Abundance (wt.%)
				a (Å)	b (Å)	c (Å)	
As-cast Mg_6Ag R_{wp} = 10.84%, S = 2.82	Mg	$P6_3/mmc$	3.02	3.2131(5)		5.2124(8)	37
	Mg_4Ag	$P6_3/m$	3.83	12.4045(3)		14.3264(6)	32
	$Mg_{54}Ag_{17}$	$Immm$	3.48	14.2367(1)	14.1994(2)	14.6703(5)	31
Hydrogenated Mg_6Ag R_{wp} = 8.97%, S = 2.74	MgH_2	$P4_2/mnm$	2.55	4.5163(6)		3.0213(4)	55
	MgAg	$Pm\text{-}3m$	1.89	3.3232(5)			45
Dehydrogenated Mg_6Ag R_{wp} = 11.32%, S = 3.14	Mg	$P6_3/mmc$	2.84	3.2127(1)		5.2129(2)	35
	Mg_4Ag	$P6_3/m$	4.67	12.4038(5)		14.3241(2)	32
	$Mg_{54}Ag_{17}$	$Immm$	3.21	14.2374(3)	14.2024(1)	14.6697(4)	33
As-cast $Mg_{5.7}In_{0.3}Ag$ R_{wp} = 6.22%, S = 1.28	Mg(In)	$P6_3/mmc$	0.77	3.2012(2)		5.2026(5)	40
	Mg_3Ag	$Fm\text{-}3$	0.66	17.6201(4)			60
Hydrogenated $Mg_{5.7}In_{0.3}Ag$ R_{wp} = 9.03%, S = 2.38	MgH_2	$P4_2/mnm$	1.08	4.5172(4)		3.0201(7)	42
	(Mg, In)Ag	$Pm\text{-}3m$	1.25	3.3101(2)			58
Dehydrogenated $Mg_{5.7}In_{0.3}Ag$ R_{wp} = 8.70%, S = 2.32	Mg	$P6_3/mmc$	1.83	3.2097(1)		5.2094(3)	28
	$(Mg, In)_3Ag$	$Fm\text{-}3$	2.42	17.6085(8)			72

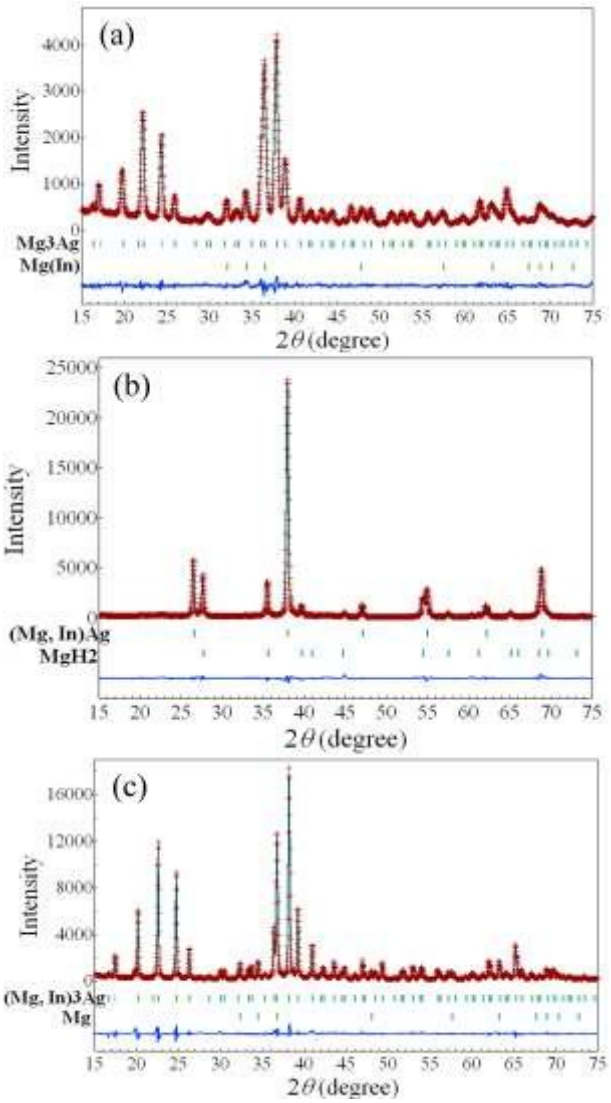

Figure 2 Rietveld refinement results of the observed XRD patterns for the (a) as-cast, (b) hydrogenated and (c) dehydrogenated $Mg_{5.7}In_{0.3}Ag$ samples at 350 °C.

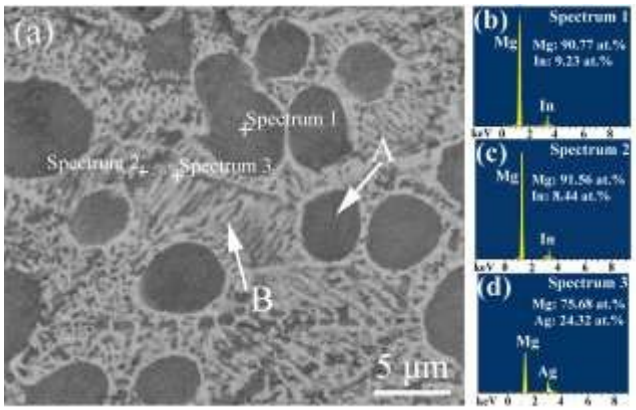

Figure 3 (a) SEM image of the as-cast $Mg_{5.7}In_{0.3}Ag$ alloy and corresponding EDS spectra of (b) pro-eutectic Mg(In) and eutectic (c) Mg(In) + (d) Mg_3Ag.

Table 2 Atomic coordinates (x, y, z), occupation factors (g) and isotropic thermal parameters (B) refined from X-ray powder diffraction data for the (Mg, In)Ag phase in the hydrogenated $Mg_{5.7}In_{0.3}Ag$ sample.

Atom	Site	g	x	y	z	B
Mg1/In1	1*b*	0.73/0.27(4)	0.5	0.5	0.5	1.6(4)
Ag1	1*a*	1	0	0	0	0.3(2)

Figure 2b shows the XRD pattern and Rietveld analysis result for the $Mg_{5.7}In_{0.3}Ag$ sample after the initial hydrogenation at 350 °C. Clearly, the hydrogenated sample was composed of MgAg and MgH_2. Because In atoms cannot dissolve in the MgH_2 lattice,[16–18,23] the In atoms dissolved in MgAg to form (Mg, In)Ag, as confirmed by XRD refinement. As listed in Table 2, ~27% of Mg1 sites are occupied by In atoms. This means that In atoms transferred from the Mg(In) solid solution to MgAg during hydrogenation. After dehydrogenation at 350 °C, the sample was composed of Mg and Mg_3Ag (Figure 2c); however, the quantity of the Mg_3Ag phase increased by 12 wt.% relative to the quantity of the as-cast sample (see Table 1). This indicates that solid MgH_2 partially reacted with (Mg, In)Ag, forming $(Mg, In)_3Ag$ and that additional MgH_2 directly decomposed to form Mg during dehydrogenation. Because of their strong affinity to Mg–Ag compounds, In atoms did not diffuse into Mg during dehydrogenation. Table 3 lists the refined atomic coordinates,

occupation number and isotropic thermal parameters for the (Mg, In)$_3$Ag phase, which show that In atoms preferentially occupied Mg1 (96*i*) and Mg3 (32*f*) sites.

On the basis of the aforementioned results, the initial hydrogenation and dehydrogenation of the $Mg_{5.7}In_{0.3}Ag$ alloy may be described as follows:

$$Mg(In) + Mg_3Ag + H_2 \rightarrow MgH_2 + (Mg, In)Ag \quad (3)$$

$$MgH_2 + (Mg, In)Ag \rightarrow Mg + (Mg, In)_3Ag + H_2 \quad (4)$$

Note that, after one de-/re-hydrogenation cycle, In atom was demonstrated to dissolve into Mg_3Ag by froming (Mg, In)$_3$Ag rather than transfer back to Mg. To further clarify it, this powder sample was examined by transimission electron microscope (TEM). Unfortunately, TEM experiments were unsuccessful due to oxidation of the sample. Hence, we tried to explain this phenomenon from the viewpoint of thermodynamics. By the Miedema semi-empirical model, the formation enthalpy of Mg(In) solid solution was calculated to be –0.7 kJ mol^{-1}.[16,26,27] However, this model can not be used to accurately quantify the formation enthalpy value of (Mg, In)$_3$Ag. Nevertheless, the effect of the dissolving In on the formation enthalpy of Mg_3Ag can be predicted qualitatively by considering the changes of size-mismatch energy and hybridization energy according to Miedema theroy.[27] Because of a very close atomic radius between Mg (0.16 nm) and In (0.157 nm), a positive contribution of size-mismatch energy to the formation enthalpy of (Mg, In)$_3$Ag can be reasonably neglected. However, a negative contribution can be induced by the increased p-d hybridization due to the subsitution of In (electron configuration: $4d^{10}5s^25p^1$) for Mg (electron configuration: $3s^2$).[27] So the formation enthalpy of (Mg, In)$_3$Ag can be deduced to be more negative than –119 kJ mol^{-1} of Mg_3Ag that was calculated based on the reaction of Eq. (1) and the standard formation enthalpies of MgH_2 and MgAg (–37 kJ mol^{-1})[28]. Thus the formation enthalpy of (Mg, In)$_3$Ag is greatly lower than that of Mg(In) solid solution. As well known that the more negative the formation enthalpy, the more favorable the formation of alloy, which may explain why In atoms prefer to dissolve into Mg_3Ag rather than Mg after dehydrogenation.

Table 3 Atomic coordinates (*x*, *y*, *z*), occupation factors (*g*) and isotropic thermal parameters (*B*) refined from X-ray powder diffraction data for the (Mg, In)$_3$Ag phase in the dehydrogenated $Mg_{5.7}In_{0.3}Ag$ sample.

Atom	Site	*g*	*x*	*y*	*z*	*B* (Å^2)
Mg1/In1	96*i*	0.84/0.16(3)	0.0993(2)	0.2599(5)	0.1571(8)	0.3(2)
Mg2/Ag2	48*h*	0.88/0.12(4)	0	0.0909(3)	0.3616(5)	0.6(5)
Mg3/In3	32*f*	0.87/0.13(2)	0.0921(4)	0.1041(1)	0.0887(6)	2.4(7)
Mg4	24*e*	1	0.2143(6)	0	0	0.6(3)
Mg5/Ag5	8*c*	0.74/0.26(3)	0.25	0.25	0.25	0.3(3)
Ag1	48*h*	1	0	0.1582(6)	0.2244(3)	0.1(6)
Ag3	4*b*	1	0.5	0.5	0.5	0.5(4)
Ag4	4*a*	1	0	0	0	0.9(2)

3.2 Hydrogen absorption/desorption mechanisms on the activated samples.

P–*C* isotherms of the activated Mg_6Ag and $Mg_{5.7}In_{0.3}Ag$ samples at 300 °C are shown in Figure 4, where the *P*–*C* isotherm of pure Mg milled for 20 h is also presented for comparison. In contrast to pure Mg, which produced one plateau in the hydrogen absorption/desorption isotherm, the Mg_6Ag and $Mg_{5.7}In_{0.3}Ag$ samples produced two plateaus, implying that the routes of their absorption/desorption reactions consisted of multiple steps instead of just one. To reveal the detailed hydrogen absorption/desorption mechanisms, XRD measurements were carried out at various stages of the absorption/desorption processes, as shown in Figure 4. XRD patterns are shown in Figure 5, and the phase abundances refined by the Rietveld method are listed Table 4. When the hydrogen pressure was 0.26 MPa (denoted as BA2), the hydrogenated Mg_6Ag sample contained MgH_2, Mg_3Ag and $Mg_{54}Ag_{17}$ (see Figure 5a and Table 4), indicating that Mg underwent hydrogenation to MgH_2 and that Mg_4Ag transformed into MgH_2 and Mg_3Ag at the lower hydrogen absorption plateau. The equilibrium pressures of these two hydrogenation reactions are very close. Upon further increase of the hydrogen pressure to 3.98 MPa (denoted as BA3), the completely hydrogenated sample was composed of MgH_2 and MgAg. This means that both Mg_3Ag and $Mg_{54}Ag_{17}$ were hydrogenated into MgH_2 and MgAg at the higher plateau for the hydrogen absorption and that the reactions had similar equilibrium pressures. Similarly, the XRD patterns of the hydrogen desorption samples (denoted as BD2 and BD3) show that desorption followed the reverse process of absorption. Therefore, the hydrogen absorption/desorption reactions may be summarized as follows:

Lower plateau: $Mg + H_2 \leftrightarrow MgH_2$ (5)

and $Mg_4Ag + H_2 \leftrightarrow MgH_2 + Mg_3Ag$ (6)

Higher plateau: Eq. (1)

and $Mg_{54}Ag_{17} + 37H_2 \leftrightarrow 37MgH_2 + 17MgAg$ (7)

Because the activated $Mg_{5.7}In_{0.3}Ag$ sample only contained the Mg and (Mg, In)$_3$Ag phases, its hydrogen absorption/desorption reactions were relatively simple. The Rietveld refinement results of the XRD patterns for the partially and fully hydrogenated/dehydrogenated $Mg_{5.7}In_{0.3}Ag$ samples (denoted as TA2, TD2, TA3 and TD3) clearly indicate that the absorption/desorption process was also accompanied by two-step reversible reactions (Figure 5b and Table 4) and that the hydrogen absorption/desorption reactions at the lower and higher

plateaus correspond to Eqs. (5) and (8), respectively.

$$(Mg, In)_3Ag + 2H_2 \leftrightarrow 2MgH_2 + (Mg, In)Ag \quad (8)$$

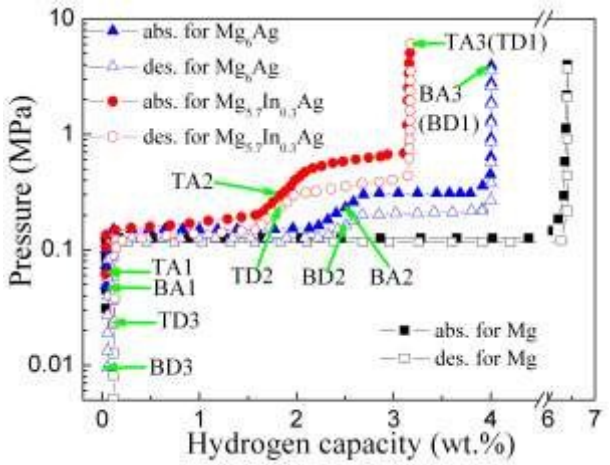

Figure 4 Pressure–composition isotherms for the activated Mg, Mg_6Ag, and $Mg_{5.7}In_{0.3}Ag$ samples at 300 °C.

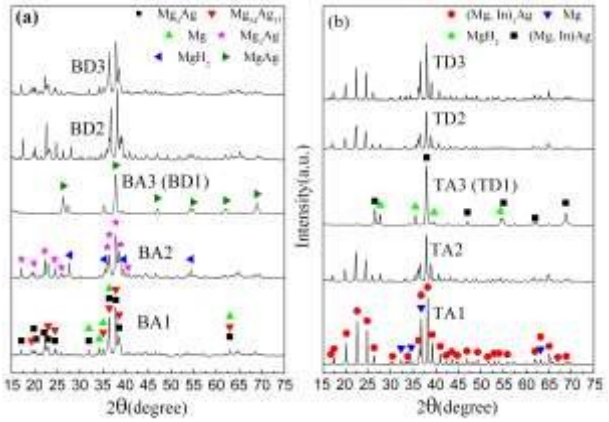

Figure 5 XRD patterns for the activated (a) Mg_6Ag and (b) $Mg_{5.7}In_{0.3}Ag$ samples under the various states indicated in Figure 4.

Table 4 Phase abundance of the activated Mg_6Ag and $Mg_{5.7}In_{0.3}Ag$ samples under the various states indicated in Figure 4.

Sample		Phase abundance (wt.%)					
		Mg	MgH_2	Mg_4Ag	$Mg_{54}Ag_{17}$	Mg_3Ag/(Mg, In)$_3Ag$	MgAg/(Mg, In)Ag
	BA1	35		32	33		
	BA2		38		34	28	
Mg_6Ag	BA3 (BD1)		53				47
	BD2		34		35	31	
	BD3	36		30	34		
	TA1	28				72	
	TA2		30			70	
$Mg_{5.7}In_{0.3}Ag$	TA3 (TD1)		43				57
	TD2	3	25			72	
	TD3	27				73	

3.3 Thermodynamic features and dual destabilization in the thermodynamics of the (Mg, In)$_3$Ag–H_2 system.

DSC curves for hydrogenated Mg, Mg_6Ag and $Mg_{5.7}In_{0.3}Ag$ samples during heating at a rate of 2 °C min^{-1} are compared in Figure 6. Only one endothermic peak (at ~367 °C) that corresponds with the dehydrogenation of the hydrogenated Mg sample was observed. However, two endothermic peaks were observed for both the hydrogenated Mg_6Ag and $Mg_{5.7}In_{0.3}Ag$ samples. For the hydrogenated $Mg_{5.7}In_{0.3}Ag$ sample, the first and second peaks at 292 and at 319 °C, respectively, indicate a hydrogen desorption reaction between (Mg, In)Ag and $2MgH_2$ (i.e., the (Mg, In)$_3$Ag–H_2 system) and hydrogen desorption from additional MgH_2, respectively. This result further confirms that in contrast to the hydrogenated Mg_6Ag sample, the (Mg, In)$_3$Ag–H_2 system was less stable and catalyzed the hydrogen desorption from additional MgH_2.

Figure 7a shows the *P–C* isotherms of the activated Mg_6Ag sample obtained at 280, 300 and 320 °C. As described in section 3.2, the lower and higher plateaus correspond to the hydrogen absorption/desorption processes of Mg_4Ag/Mg and $Mg_{54}Ag_{17}$/Mg_3Ag, respectively. Thus, the thermodynamic properties of the hydrogen storage by Mg and Mg_3Ag may be calculated from van't Hoff plots (see Figure 7c). Accordingly, the ΔH_d and the entropy change (ΔS_d) of the hydrogen desorption for the Mg–H_2 system were found to be 75.5 kJ mol^{-1} H_2 and 133.8 J K^{-1} mol^{-1} H_2, respectively; those same values for the Mg_3Ag–H_2 system were found to be 71.8 kJ mol^{-1} H_2 and 131.3 J K^{-1} mol^{-1} H_2, respectively (see Table 5). Similarly, the hydrogen storage thermodynamics of Mg and (Mg, In)$_3$Ag in the $Mg_{5.7}In_{0.3}Ag$

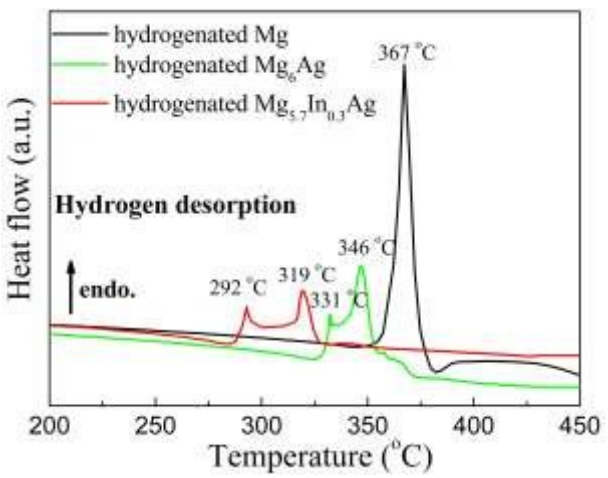

Figure 6 DSC curves for the hydrogenated Mg, Mg_6Ag, and $Mg_{5.7}In_{0.3}Ag$ samples.

sample may also be determined from their *P*–*C* isotherms (Figure 7b). ΔH_d values of the Mg–H_2 and (Mg, In)$_3$Ag–H_2 systems are 74.9 and 62.6 kJ mol^{-1} H_2, respectively. Evidently, the ΔH_d value of the (Mg, In)$_3$Ag–H_2 system further decreased, although the thermodynamics of the Mg–H_2 system was unchanged. As mentioned in section 3.1, In could transfer from the Mg(In) solid solution into (Mg, In)Ag during the first hydrogenation and could not diffuse back to Mg in subsequent dehydrogenation. Therefore, the hydrogen storage thermodynamics of Mg in the $Mg_{5.7}In_{0.3}Ag$ sample after activation was not influenced by In, but the thermodynamics of (Mg, In)$_3$Ag was improved because of the dissolved indium.

Table 5 Enthalpy and entropy changes of hydrogen desorption from the Mg, Mg_6Ag and $Mg_{5.7}In_{0.3}Ag$ samples.

Sample	Mg	Mg_6Ag		$Mg_{5.7}In_{0.3}Ag$	
		low plateau	high plateau	low plateau	high plateau
ΔH_d (kJ mol^{-1} H_2)	76	75.5	71.8	74.9	62.6
ΔS_d (J K^{-1} mol^{-1} H_2)	134	133.8	131.3	133.	125.8

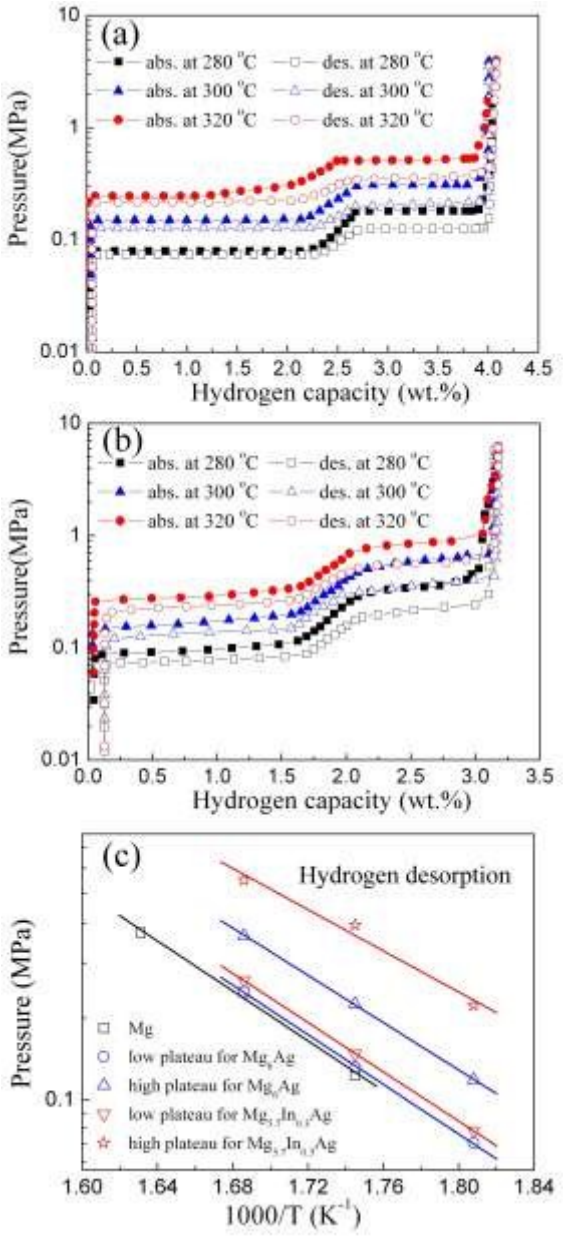

Figure 7 Pressure–composition isotherms for the activated (a) Mg_6Ag and (b) $Mg_{5.7}In_{0.3}Ag$ samples at 280, 300 and 320 °C. (c) van't Hoff plots for hydrogen desorption on the Mg, Mg_6Ag, and $Mg_{5.7}In_{0.3}Ag$ samples.

3.4. Kinetic properties and catalytic effect of (Mg, In)$_3$Ag on hydrogen desorption from MgH_2.

Figure 8 presents kinetic curves for hydrogen absorption and desorption on the activated samples at 260 °C. It can be seen that absorption on the Mg_6Ag and $Mg_{5.7}In_{0.3}Ag$ samples were completed within 20 and 15 min, respectively (see Figure 8a). After complete absorption (see Figure 8b), hydrogen could completely desorb from the Mg_6Ag and $Mg_{5.7}In_{0.3}Ag$ samples within 55 and 25 min, respectively. This indicates that the kinetics on both the Mg_3Ag phase and the dissolved In were enhanced.

To reveal the controlling step for the hydrogen desorption, isothermal curves (Figure 9) were analyzed by using a kinetic model (Eq. (9)):

$$g(a) = \int d\alpha / f(\alpha) = kt \qquad (9)$$

where α is the reaction fraction at the desorption time t, $g(\alpha)$ and $f(\alpha)$ are the functions representing the specific reaction mechanism, and k is the rate constant. Various mechanism functions reported in Refs. 29–31 were used to fit the experimental data shown in Figure 9. The function $1-(1-\alpha)^{1/2}$ gave the best linearity over a broader range of α values for each measurement (correlation coefficient R^2 of >0.995). Linear relationships between $1-(1-\alpha)^{1/2}$ and t (Figure 10) indicate that the hydrogen desorption processes on the Mg_6Ag and $Mg_{5.7}In_{0.3}Ag$ samples in the experimental temperature range were mainly controlled by two-dimensional phase-boundary migration.

Rate constants at different temperatures were obtained from the slopes of the fitted straight lines shown in Figure 10. The apparent activation energy (E_a) for the hydrogen desorption could thus be determined according to the Arrhenius equation:

$$k = k_0 \exp[-E_a/(RT)] \qquad (10)$$

where k_0 is the pre-exponential factor and R is the gas constant. Arrhenius plots for the hydrogen desorption are illustrated in Figure 11. E_a values of the hydrogenated Mg_6Ag and $Mg_{5.7}In_{0.3}Ag$ samples calculated from the slopes ($-E_a/R$) of the straight lines are 89.8 and 78.2 kJ mol^{-1}, respectively. These values are much lower than that of pure MgH_2 (160–170 kJ mol^{-1}),[32,33] and thus indicate enhanced hydrogen desorption kinetics due to the combination of Mg_3Ag or (Mg, In)$_3$Ag. These enhanced kinetic properties can be understood two aspects as follow: (i) many studies have confirmed that the non-hydride forming elements exhibit a beneficial effect upon the hydrogen desorption of MgH_2 based on the fact that their *d*-electrons can interact with the hydrogen anti-bonding orbital and weaken the Mg–H bonds.[34–37] Similarly, in this study the formation of Mg–Ag bonds also destabilize the Mg–H bonds by prompting neighboring electron transfer between Mg and H atoms;[36,37] (ii)

the substitution of In for Mg increases the concentration of non-hydride forming elements, thus resulting in more destabilized effect on Mg–H bonds. Moreover, In atom prones to be rich in the interfaces of MgH_2 and $(Mg, In)_3Ag$, which provides preferred sites for dissociation/ recombination of hydrogen atoms.[23,38,39]

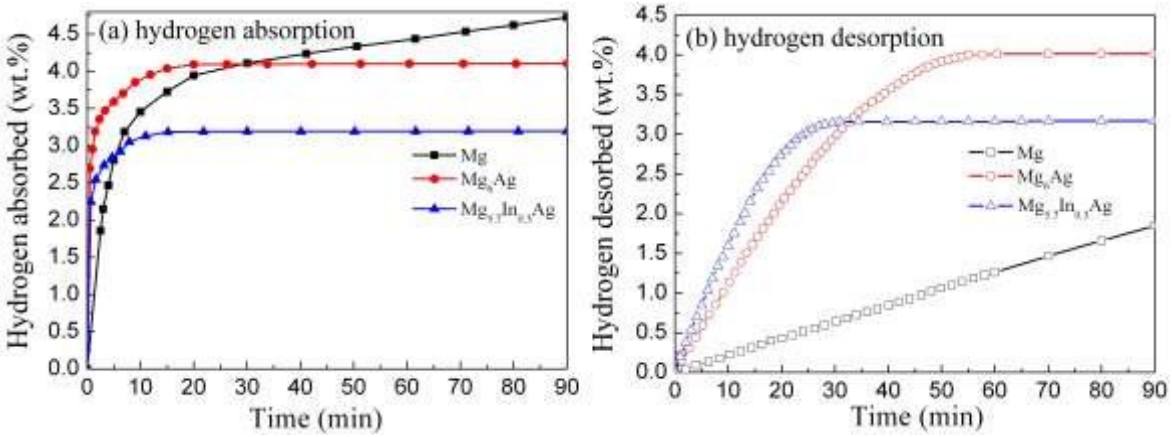

Figure 8 Kinetic curves for (a) hydrogen absorption and (b) hydrogen desorption on the activated Mg_6Ag and $Mg_{5.7}In_{0.3}Ag$ samples at 260 °C.

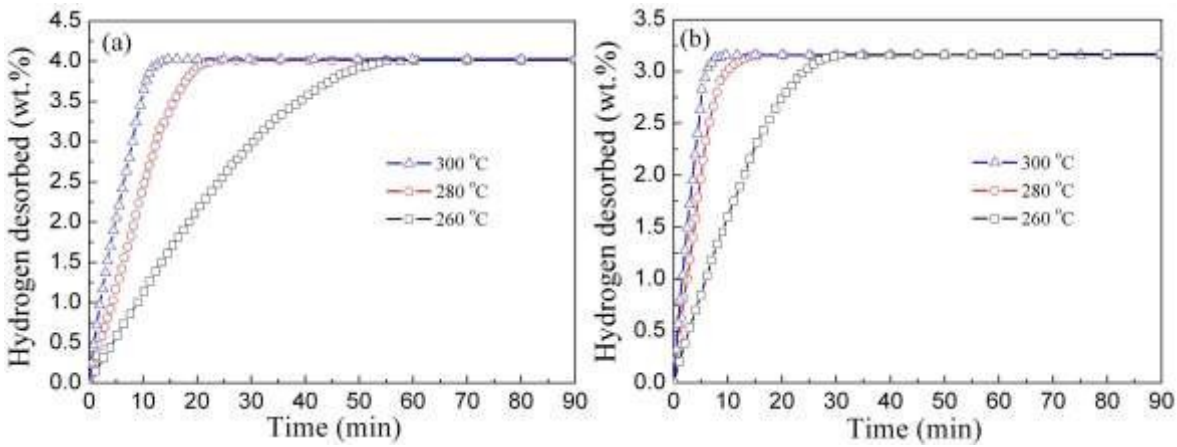

Figure 9 Isothermal hydrogen desorption curves for the (a) Mg_6Ag and (b) $Mg_{5.7}In_{0.3}Ag$ samples.

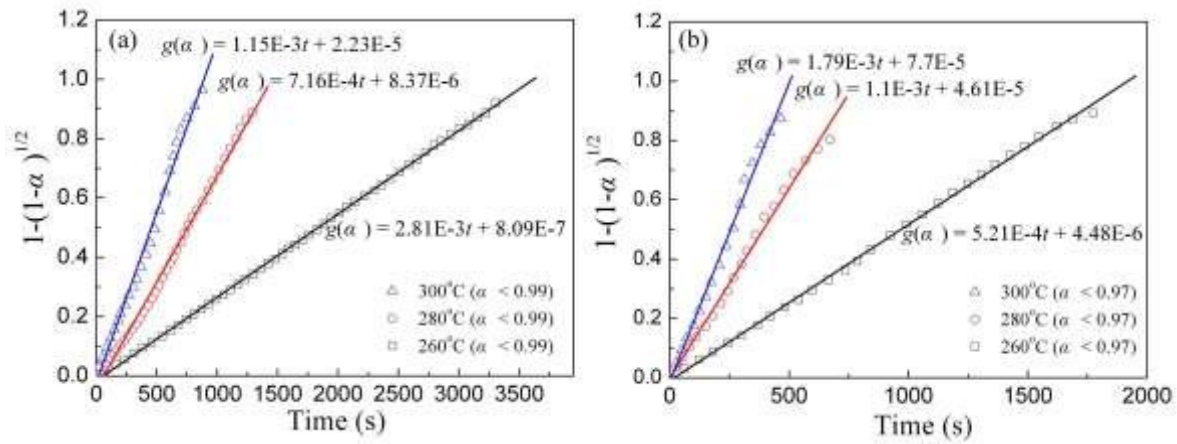

Figure 10 Plots of $1 - (1 - \alpha)^{1/2}$ vs. t for the hydrogenated (a) Mg_6Ag and (b) $Mg_{5.7}In_{0.3}Ag$ samples.

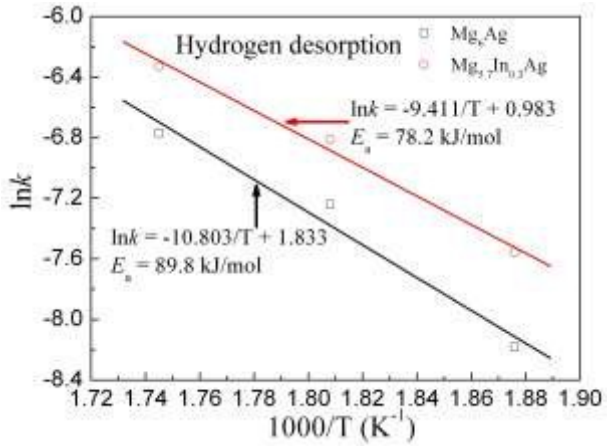

Figure 11 Arrhenius plots for the hydrogen desorption from the Mg_6Ag and $Mg_{5.7}In_{0.3}Ag$ samples.

4 Conclusions

The hydrogen storage mechanisms and properties of the $Mg_{5.7}In_{0.3}Ag$ and Mg_6Ag alloys were comparatively studied in the present work. The principal conclusions may be summarized as follows: (i) Different from a Mg(In) solid solution and Mg_3Ag in the as-cast $Mg_{5.7}In_{0.3}Ag$ alloy, which transformed into Mg and (Mg, In)$_3$Ag after the initial hydriding/dehydriding process (i.e., activation), the as-cast Mg_6Ag alloy was composed of Mg, Mg_4Ag, and $Mg_{54}Ag_{17}$ phases. (ii) Both activated Mg_6Ag and $Mg_{5.7}In_{0.3}Ag$ samples produced isotherms with two plateaus corresponding to hydrogen absorption/desorption steps. The lower and higher plateaus of Mg_6Ag correspond to the hydrogen absorption/desorption processes on Mg/Mg_4Ag and $Mg_3Ag/Mg_{54}Ag_{17}$, respectively; those of $Mg_{5.7}In_{0.3}Ag$ correspond to the absorption/desorption processes on Mg and (Mg, In)$_3$Ag, respectively. Our comparative study confirmed that the (Mg, In)$_3$Ag–H_2 system had altered thermodynamics (ΔH_d = 62.6 kJ mol^{-1} H_2), which could be ascribed to the dual destabilization of Ag alloying and the dissolution of In. (iii) The solid solution of In enhanced the catalytic effect of (Mg, In)$_3$Ag on hydrogen desorption from additional MgH_2. As it possessed a reduced activation energy (78.2 kJ mol^{-1}), the hydrogen desorption from the $Mg_{5.7}In_{0.3}Ag$ sample showed kinetics that was faster than that of the desorption from the Mg_6Ag sample.

Acknowledgments

This work was financially supported by the National Natural Science Foundation of China Project Nos. 51271002, 51431001, 51271078 and U120124, by GDUPS (2014) and by KLGHEI (KLB11003).

Notes and references

[a]*School of Materials Science and Engineering, Anhui University of Technology, Maanshan, 243002, China. E-mail: qazhang_ahut@163.com ; Tel. & Fax: +86-555-2311570*

[b]*Department of Materials Science, Fudan University, Shanghai, 200433, China.*

[c]*School of Materials Science and Engineering, South China University of Technology, Guangzhou, 510641, China. E-mail: meouyang@scut.edu.cn; Tel: +86-20-87112762*

[d]*Key Laboratory of Advanced Energy Storage Materials of Guangdong province, South China University of Technology, Guangzhou 510641, P.R. China.*

1 L. Schlapbach and A. Züttel, *Nature*, 2001, **414**, 353−358.
2 Y. Song, Z. X. Guo and R. Yang, *Phys. Rev. B.*, 2004, **69**, 094205.1–11.
3 M. Dornheim, S. Doppiu, G. Barkhordarian, U. Boesenberg, T. Klassen, O. Gutfleisch and R. Bormann, *Scripta Mater.*, 2007, **56**, 841–846.
4 M. Paskevicius, D. A. Sheppard and C. E. Buckley, *J. Am. Chem. Soc.*, 2010, **132**, 5077–5083.
5 T. R. Jensen, A. Andreasen, T. Vegge, J. W. Andreasen, K. Stahl, A. S. Pedersen, M. M. Nielsen, A. M. Molenbroek and F. Besenbacher, *Int. J. Hydrogen Energy*, 2006, **31**, 2052–2062.
6 I. P. Jain, C. Lal and A. Jain, *Int. J. Hydrogen Energy*, 2010, **35**, 5133–5144.
7 G. S. Walker, M. Abbas, D. M. Grant and C. Udeh, *Chem. Commun.*, 2011, **47**, 8001–8003.
8 J. J. Reilly and R. H. Wiswall, *Inorg. Chem.*, 1967, **6**, 2220–2223.
9 J. J. Reilly and R. H. Wiswall, *Inorg. Chem.*, 1968, **7**, 2254–2256.
10 G. I. Duarte, L. A. C. Bustamante and P. E. V. Miranda, *Scripta Mater.*, 2007, **56**, 789–792.
11 A. Andreasen, *Int. J. Hydrogen Energy*, 2008, **33**, 7489–7497.
12 J. C. Crivello, T. Nobuki, S. Kato, M. Abe and T. Kuji, *J. Alloys Compd.*, 2007, **446–447**, 157–161.
13 T. Z. Si, J. B. Zhang, D. M. Liu and Q. A. Zhang, *J. Alloys Compd.*, 2013, **581**, 246–249.
14 H. C. Zhong, H. Wang and L. Z. Ouyang, *Int. J. Hydrogen Energy*, 2014, **39**, 3320–3326.
15 J. C. Crivello, T. Nobuki and T. Kuji, *Int. J. Hydrogen Energy*, 2009, **34**, 1937–1943.
16 H. C. Zhong, H. Wang, J. W. Liu, D. L. Sun and M. Zhu, *Scripta Mater.*, 2011, **65**, 285–287.
17 C. S. Zhou, Z. Z. Fang, J. Lu and X. Y. Zhang, *J. Am. Chem. Soc.*, 2013, **135**, 10982−10985.
18 F. P. Luo, H. Wang, L. Z. Ouyang, M. Q. Zeng, J. W. Liu and M. Zhu, *Int. J. Hydrogen Energy*, 2013, **38**, 10912–10918.
19 L. Z. Ouyang, Z. J. Cao, H. Wang, J. W. Liu, D. L. Sun, Q. A. Zhang and M. Zhu, *Int. J. Hydrogen Energy*, 2013, **38**, 8881–8887.
20 Q. A. Zhang, D. D. Liu, Q. Q. Wang, F. Fang, D. L. Sun, L. Z. Ouyang and M. Zhu, *Scripta Mater.*, 2011, **65**, 233–236.
21 W. J. Song, J. S. Li, T. B. Zhang, H. C. Kou and X. Y. Xue, *J. Power Sources*, 2014, **245**, 808–815.
22 J. Cermak and L. Kral, *J. Power Sources*, 2012, **197**, 116–120.
23 J. Cermak and L. Kral, *J. Power Sources*, 2012, **214**, 208–215.
24 T. Liu, Y. R. Cao, C. G. Qin, W.S. Chou and X. G. Li, *J. Power Sources*, 2014, **246**, 277–282.
25 F. Izumi and T. Ikeda, *Mater. Sci. Forum*, 2000, **321–323**, 198–203.
26 A. R. Miedema, P. F. De Chatel and F. R. De Boer, *Phys. B*, **1980**, 100, 1–28.
27 F. R. De Boer, R. Boom, W. C. M. Mattens, A. R. Miedema and A. K. Niessen, *Cohesion in metals: Transition metal alloys*, North-Holland, Amsterdam, 1988.
28 G. Urretavizcaya,A. C. S. Chavez and F. J. Castro, *J. Alloys Compd.*, 2014, **611**, 202–209.
29 Y. F. Liu, K. Zhong, K. Luo, M. X. Gao, H. G. Pan and Q. D. Wang, *J. Am. Chem. Soc.*, 2009, **131**,1862–1870.
30 Y. T. Li, G. Y. Zhou, F. Fang, X. B. Yu, Q. A. Zhang, L. Z. Ouyang, M. Zhu and D. L. Sun, *Acta Mater.*, 2011, **59**, 1829–1838.
31 G. Barkhordarian, T. Klassen and R. Bormann, *J. Alloys Compd.*, 2006, **407**, 249–255.
32 A. Andreasen, T. Vegge and A. S. Pedersen, *J. Phys. Chem. B*, 2005, **109**, 3340–3344.
33 M. H. Mintz and Y. Zeiri, *J. Alloys Compd.*, 1994, **216**, 159–175.
34 G. Liang, J. Huot, S. Boily, A. Van Neste and R. Schulz, *J. Alloys Compd.*, 1999, **292**, 247–252.
35 Y. Fu, M. Groll, R. Mertz and R. Kulenovic, *J. Alloys Compd.*, 2008, **460**, 607–613.

36 Y. Jia, C. H. Sun, L. Cheng, M. A. Wahab, J. Cui, J. Zou, M. Zhu and X. D. Yao, *Phys. Chem. Chem. Phys.*, 2013, **15**, 5814–5820.
37 Y. Jia, C. H. Sun, S. H. Shen, J. Zou, S. S. Mao and X. D. Yao, *Renewable and Sustainable Energy Reviews*, 2015, **44**, 289–303.
38 M. Au, J. Wu and Q. D. Wang, *Int. J. Hydrogen Energy*, 1995, **20**, 141–150.
39 Z. Gavra, Z. Hadri and M. H. Hintz, *J. Inorg. Nucl. Chem.*, 1981, **43**, 1763–1768.

For Table of Contents Only

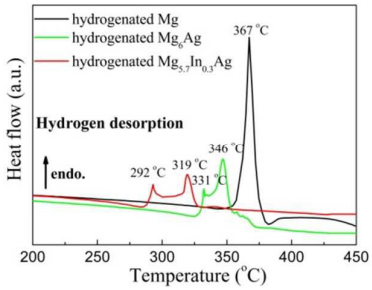

Both thermodynamics and kinetics of the $Mg_{5.7}In_{0.3}Ag–H_2$ system were significantly destabilized by combining Ag alloying with In dissolution.